# Wind Velocity Effect on the Aerodynamic and Acoustic Behavior of a Vertical Axis Wind Turbine

MEROUANE HABIB
Department of Mechanical Engineering,
University of Mascara,
ALGERIA

*Abstract*: - In this work we present a numerical study on the effect of wind velocity on the aerodynamic and acoustic behavior of a Savonius-type vertical axis wind turbine (VAWT). The study focuses on the prediction of the torque coefficient for different flow velocities and rotational velocities of the wind turbine. We also present the triggering of the wake zone near the wind turbine blades to see the dynamic effect on the behavior of the wind turbine. The study of the numerical simulation is carried out using a fluent CFD calculation code using the finite volume method for the discretization of the differential equations. The equations governing the flow are solved by the SIMPLE algorithm using two K-epsilon turbulence models.

*Key-Words:* - Wind turbine; Savonius turbine; Aerodynamics wind turbine; wind turbine sound, vertical axis turbine; Aero-acoustic.

Received: March 15, 2023. Revised: February 7, 2024. Accepted: March 6, 2024. Published: April 25, 2024.

## 1 Introduction

The Savonius vertical wind turbine consists of two or more blades attached directly to the vertical axis in opposite directions. The wind turbine is driven by the force of the wind which turns the rotor by producing mechanical energy that can be transformed into electrical energy through a generator.

With its simplicity, the Savonius vertical wind turbine fits into the roofs of buildings without altering their aesthetics. It can also be installed at the top of a mast. Discreet and silent, it works even in light winds, but remains unsuitable for producing large amounts of electricity. The Savonius wind turbine has many variations, including a very fashionable helical version that optimizes wind resistance.

The Savonius wind turbine works on the principle of differential drag: the convex part has a drag force (force opposing the movement of the wind) less than the drag force of the concave part. This difference between the forces creates a torque that turns the wind turbine.

The Savonius wind turbines type are generally used in domestic buildings to produce electrical energy and can also be used in a hybrid system with artificial intelligence (solar panel-Savonius wind turbine) to operate small power machines such as pumping water in agricultural areas

Many researchers have extensively studied the performance of vertical-axis wind turbines through experimental and numerical studies, [1], [2], [3], [4], [5], [6], [7] [8], [9].

The authors [10], studied by experiment in a Wind Tunnel the performance of a Savonius Rotor in the flow field. His study describes the experimental evaluation of the unsteady flow field downstream the rotor using a constant temperature hot wire Anemometer (CTA). Whilst, for performance analysis. The torque measurements have been obtained directly from the Servo Amplifier torque monitor. They indicate that the torque coefficient depends linearly with the tip velocity ratio, with the highest value at the lowest $\lambda$

The authors [11], have investigated experimentally and numerically the flow around a vertical axis Savonius- type wind turbine. The rotor has two blades and a height that is approximately equal to the diameter of the rotor. His results confirm the ability of the modeling of detached vortex simulations to represent the turbulent detached flow well. Thus, this type of turbulence modeling can be applied to analyze and optimize the Savonius wind turbine as well as another drag-type wind turbine.

The results obtained for the power coefficient show that they are very close to the experimental data.

The performance of the axial wind turbine is studied by experiment with different types of blades two-bladed in a wind tunnel, [12]. The two-bladed turbine is tested in an open type test section and its performance is assessed in terms of power and torque coefficients. The experiments have also been conducted with other standard blades such as semi-circular, semi-elliptic, Benesh and Bach types to have a direct comparison. His investigation demonstrates that a gain of 34.8% in maximum power coefficient with the newly developed two-bladed turbine.

The authors [13], carried out a noise investigation of small-scale vertical axis wind turbines in urban areas and they observed that the process of upstroke in the windward rotor regions (20◦∼130◦) and downstroke in the leeward rotor regions (200◦ ∼ 310◦) are the main mechanisms generating noise due to the dynamic stall effect. The windward side of VAWTs constitutes a significant noise source region. With an increase in wind velocity, the effect of self-induced turbulence on the noise characteristics varies depending on the operating state of the VAWTs. According to their results, under a wind velocity of 10 m/s at night, the noise emitted by VAWTs reaches the noise control standard of some countries at distances of more than 260 m

The authors [14], presented low noise prediction for a VAWT operating at a low $Re$ number. They used the low fidelity method which is based on the actuator cylinder model coupled with semi-empirical models for airfoil self-noise and turbulence interaction noise. Their results showed good agreement between the high-fidelity simulations and the low-fidelity model at low frequencies, where turbulence interaction noise is the dominant noise source. At higher frequencies, airfoil-specific noise dominates and existing methods, based on stable airfoils, do not predict noise correctly. His work shows that the presented low-fidelity model predicts turbine aerodynamics and aeroacoustics with acceptable accuracy for a design stage. However, improvements are needed to better predict the far-field noise of blades in an unstable field

# 2 Mathematical Modelling

## 2.1 Standard k-ε Turbulence Model

The k-epsilon model is the most used for the prediction of turbulent flows. This model is based on the Boussinesq approximation. This hypothesis corresponds to relating the Reynolds stresses to the mean gradients of turbulent velocity and viscosity.

$$-\rho\overline{u_i'u_j'} = \mu_t\left(\frac{\partial\overline{u}_i}{\partial x_j}+\frac{\partial\overline{u}_j}{\partial x_i}\right)-\frac{2}{3}\rho k\delta_{ij} \tag{1}$$

Where k is the turbulent kinetic energy, defined as:

$$k = \frac{1}{2}\overline{u_i'u_i'} \tag{2}$$

Turbulent viscosity is modeled as follows:

$$\mu_t = \rho C_\mu \frac{k^2}{\varepsilon} \tag{3}$$

With ε is the dissipation rate given by:

$$\varepsilon = \frac{\mu_t}{\rho}\left(\overline{\frac{\partial u_i}{\partial u_j}\frac{\partial u_i}{\partial u_j}}\right) \tag{4}$$

For the k-epsilon model the two additional equations are given:

$$\frac{\partial}{\partial t}(\rho k)+\frac{\partial}{\partial x_i}(\rho k\,\overline{u}_i) = \frac{\partial}{\partial x_j}\left[\left(\mu+\frac{\mu_t}{\sigma_k}\right)\frac{\partial k}{\partial x_j}\right] + G_k + G_b - \rho\varepsilon - Y_M + S_k \tag{5}$$

$$\frac{\partial}{\partial t}(\rho\varepsilon)+\frac{\partial}{\partial x_i}(\rho\varepsilon\,\overline{u}_i) = \frac{\partial}{\partial x_j}\left[\left(\mu+\frac{\mu_t}{\sigma_\varepsilon}\right)\frac{\partial\varepsilon}{\partial x_j}\right] + C_{\varepsilon 1}\frac{\varepsilon}{k}(G_k + C_{\varepsilon 3}G_b) - C_{\varepsilon 2}\rho\frac{\varepsilon^2}{k} + S_\varepsilon \tag{6}$$

Where

$G_k$ and $G_b$ are the kinetic energy of turbulence due to mean velocity gradients and buoyancy, respectively.

$C_{\varepsilon 1}$, $C_{\varepsilon 2}$, and $C_{\varepsilon 3}$ are the constants given in Table 1.

$\sigma_k$ and $\sigma_\varepsilon$ are the turbulent Prandtl numbers for k and respectively given in Table 1.

$S_k$ et $S_\varepsilon$ are the source terms for k and ε respectively.

The kinetic energy of turbulence due to mean velocity gradients is modeled as:

$$G_k = -\rho\overline{u_i'u_j'}\frac{\partial u_i}{\partial x_i} \tag{7}$$

The kinetic energy of turbulence due to buoyancy is given by:

$$G_b = \beta g_i \frac{\mu_t}{Pr_t} \frac{\partial T}{\partial x_i} \quad (8)$$

Where $\beta$ is the coefficient of thermal expansion.

The coefficients of the models are given in Table 1:

Table 1. Constants of the standard k – ε model

| $C_\mu$ | $C_{\varepsilon 1}$ | $C_{\varepsilon 2}$ | $C_{\varepsilon 3}$ | $\sigma_k$ | $\sigma_\varepsilon$ |
|---|---|---|---|---|---|
| 0, 09 | 1, 44 | 1, 92 | 0.5 | 1, 0 | 1, 3 |

The coefficient of power of a wind turbine

$$C_p = \frac{p}{\frac{1}{2}\rho V^2 SR} \quad (9)$$

With P is the maximum power obtained from the wind

$$C_m = \frac{C}{\frac{1}{2}\rho V^2 SR} \quad (10)$$

$$C_p = \lambda\ C_m \quad (11)$$

With λ is the Tip speed ratio between tangential velocity from the rotor tip and the free-flow velocity of the wind

$$\lambda = \frac{\omega R}{V} \quad (12)$$

Where
$\omega$ : is the angular velocity of the rotor and R is the radius of the rotor

### 2.2 Modeling of Acoustic Waves

For the prediction of sound waves around the blades of the wind turbine, the Broadband Noise Source Models model was used for an isotropic turbulent flow whose acoustic power is determined by the following relationship:

$$P_A = \alpha \rho_0 \left(\frac{u^3}{\ell}\right) \frac{u^5}{a_0^5} \quad (13)$$

where
$u$ is turbulence velocity
$\ell$ is length scales
$a_0$ is the velocity of sound.
$\alpha$ is a model constant.

The sound field produced by the turbulent flow around a solid body for very low Mach numbers is given after Curle's integral [15] by the following relation:

$$p'(\vec{x},t) = \frac{1}{\pi a_0} \int_S \frac{(x_i - y_i) n_i}{r^2} \frac{\partial p}{\partial t}(\vec{y},\tau) ds(\vec{y}) \quad (14)$$

where
$\tau$ is the emission time
S is the integration surface
The sound intensity in the far field can be written:

$$\overline{p'^2} = \frac{1}{16\pi^2 a_0^2} \int_S \frac{cos^2}{r^2} \overline{\left[\frac{\partial p}{\partial t}(\vec{y},\tau)\right]}^2 A_c(\vec{y}) ds(\vec{y}) \quad (15)$$

where
$A_c$ is the correlation area

## 3 Grid and Computational Domain

The Savonius wind turbine is made up of two semi-cylindrical blades offset from each other by a distance **a** and **e** with diameter **D**. The various geometric parameters of the wind turbine are mentioned in the Figure. 1 The height of the blades H = 1.8 m, H/D = 1.6, e = 0.16D, a / D = 0

The mesh was carried out using the gambit software with triangular meshes and 28416 nodes; the domain of the mesh is devised in two parts, the first one with a fixed mesh and the second with a moving mesh

## 4 Boundary Condition

The boundary conditions are defined in the extremity of the computational domain, at the inlet condition a velocity flow value is imposed to (4, 6 and 8 m/s), at the outlet of the flow a atmospheric pressure is maintained, the wind turbine is limited by two walls (Wall conditions). The rotation velocity can be varied for n = 70 to 90 rpm

The wind turbine simulation domain has axial and radial distances of 16 and 10 m respectively to form a rectangle where the wind turbine is placed in its center

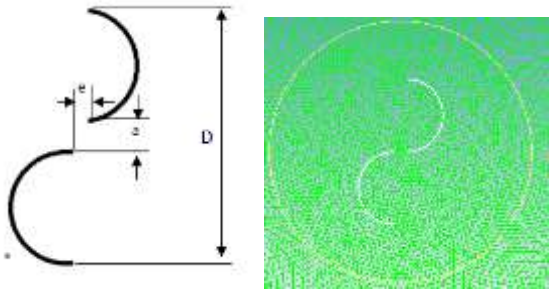


Fig. 1: Configuration of the Savonius wind turbine

## 5 Results and Discussion

In this section we present the main results obtained by numerical simulation using the k-epsilon model for the prediction of turbulence around the blades of the wind turbine and the Broadband Noise Source model for the prediction of the acoustic waves

To evaluate the performance of the wind turbine at all points of its operation, three wind velocity values were chosen (4, 6, and 8 m/s) and three times intervals of 0.2, 0.4 and 0.6 s. The wind velocity values, the corresponding angular velocities and the time steps used for each calculation are summarized in Table 2 and Table 3.

Table 2. The first step

| Wind velocity | Angular velocity | Times |
|---|---|---|
| 4 | 80 rpm | 0.2 s, 0.4 s , 0.6 s |
| 6 | | |
| 8 | | |

Table 3. The second step

| Wind velocity | Angular velocity | Times |
|---|---|---|
| 6 m/s | 70 rpm | 0.2 s, 0.4 s , 0.6 s |
| | 80 rpm | |
| | 90 rpm | |

Figure 2, Figure 3 and Figure 4 show the mean velocity field for different wind velocities (4, 6, and 8 m/s) and three calculation times (0.2, 0.4, and 0.6 s). We observe in these figures that the field of the mean velocity is important around the blades of the wind turbine mainly in the sides of the upper surface of the blade which turns in the same direction as the wind. This velocity decreases to reach zero values behind the rotor witch created by a significant depression.

Figure 5, Figure 6 and Figure 7 show the distribution of the pressure coefficient for different wind velocities (4, 6, and 8 m/s) and three calculation times (0.2, 0.4, and 0.6 s). We observe in these figures the pressure coefficient depends only on the orientation of the Savonius rotor. A very high-pressure coefficient is observed upstream of the Savonius rotor which is in opposition with the velocity wind direction in the convex part of the blade. At the concave surface of the blade, there is a strong depression which gives a very low pressure coefficient. The most important areas of depression also appear in the central region of the Savonius rotor. This depression zone extends downstream of the rotor to the exit of the domain.

Figure 8 shows the torque coefficient obtained by the numerical simulation for different flow conditions (different wind velocities 4, 6, and 8 m/s, respectively). The results indicate that the torque coefficient has a positive and a negative sign with maximum and minimum values for all different flow conditions, the torque coefficient is important when the wind velocity is higher than 8 m/s. At wind velocity equal to 8 m/s the torque coefficient is positive for the intervals angle situated between 120° to 240° and negative for the angles situated between 0° to 100°, 280° to 360°

Figure 9 presents the torque coefficient for different angular velocities of the Savonius rotor 70, 80, and 90 rpm in moderate velocity wind 6 m/s. The results indicate that the torque coefficient depends also on the angular velocity of the Savonius rotor. We observe a phase shift between the curves which can be explained by the variation in the frequency of the angular velocity

Figure 11, Figure 12 and Figure 13 show the sound power level contours for different time intervals. It is observed in these figures that the acoustic power is mainly concentrated at the level of the blades of the Savonius turbine and mainly in the upper part of the blades, this acoustic power is very low of the order of 30 dB for a very low wind velocity in occurrence for 4 m/s, the sound field increases according to the increase in wind velocity and according to the orientation of the blades of the wind turbine. We note that this acoustic power strongly depends on the angle of orientation of the blades

Table 4 and Table 5 present the statistical results of the maximum and minimum torque coefficient during the stabilized operation of the Savonius wind turbine for the case where the wind velocity is

variable from 4, 6, and 8 m/s and an angular velocity of the rotor is maintained constant 80 rpm, for the second case the wind velocity is kept constant and the angular velocity of the rotor is variable from 70, 80 and 90 rpm. We notice that the values of the maximum torque coefficients have positive signs which are important for the case where the wind velocity is 8 m/s with a value of +0.46 and for the case where the wind velocity is 6 m/s and an angular velocity of 90 rpm with a value of +0.46. We also notice that there are minimum values of the negative torque coefficients for the case where the wind velocity is 8 m/s with a value of - 0.15 and - 0 .13 for the case when the wind velocity is 6 m/s and an angular velocity of 70 rpm.

Table 4. Statistical results for the first step

| Wind velocity | Angular velocity | Maximum torque coefficient | Minimum torque coefficient |
|---|---|---|---|
| 4 | 80 rpm | + 0.25 | + 0.1 |
| 6 | | + 0.38 | + 0.04 |
| 8 | | + 0.46 | - 0.15 |

Table 5. Statistical results for the second step

| Wind velocity | Angular velocity | Maximum torque coefficient | Minimum torque coefficient |
|---|---|---|---|
| 6 m/s | 70 rpm | + 0.28 | - 0 .13 |
| | 80 rpm | + 0.38 | - 0.05 |
| | 90 rpm | + 0.46 | - 0.09 |

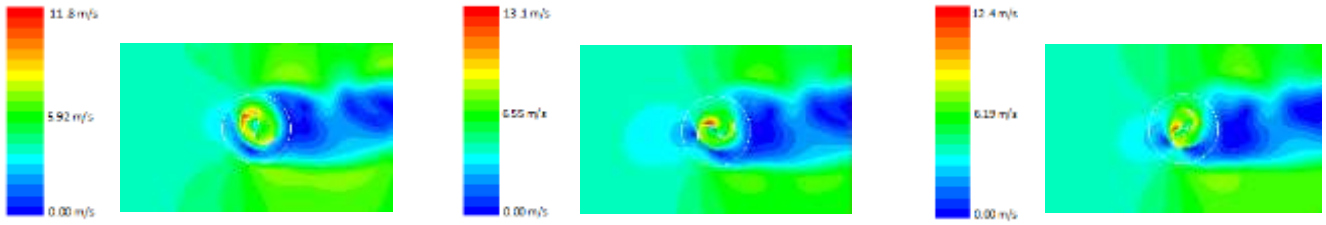

Fig. 2: The average velocity field at different calculation times for wind velocity 4 m/s

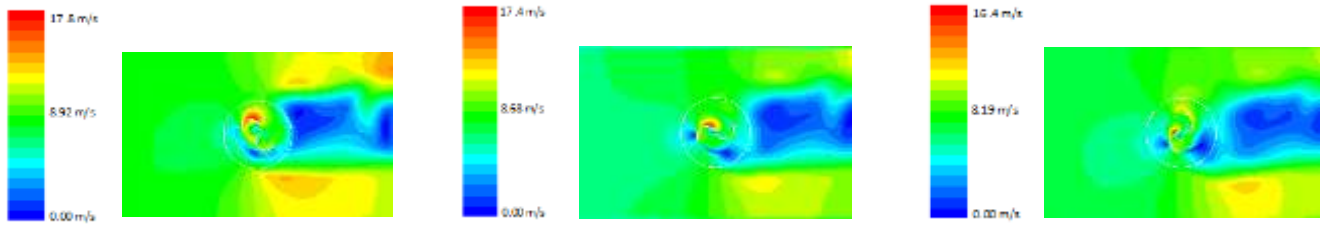

Fig. 3: The average velocity field at different calculation times for wind velocity 6 m/s

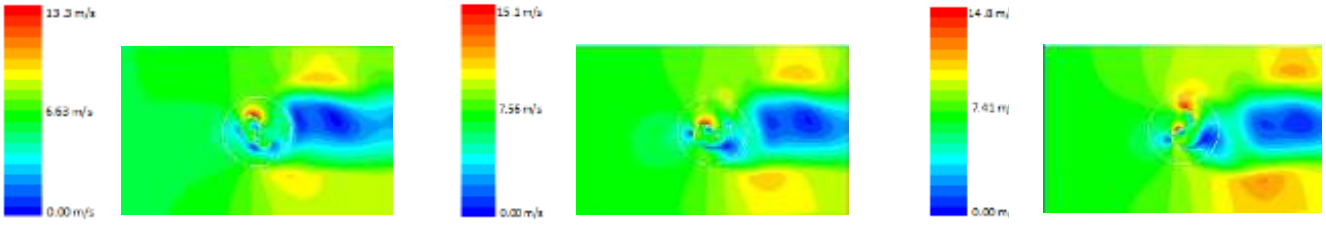

Fig. 4: The average velocity field at different calculation times for wind velocity 8 m/s

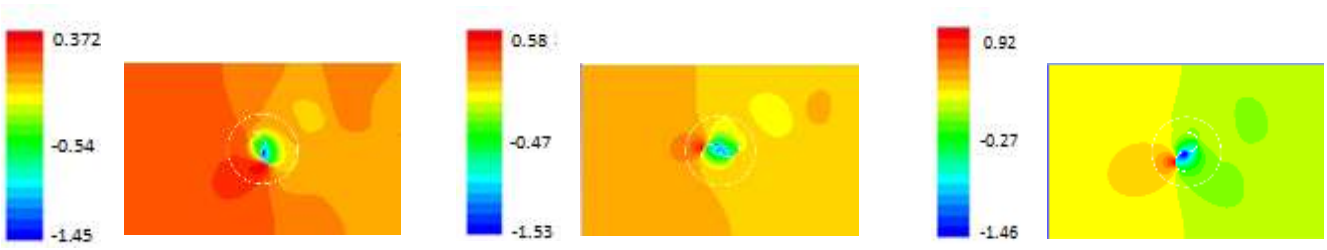


Fig. 5: The pressure coefficient at different calculation times for wind velocity 4 m/s

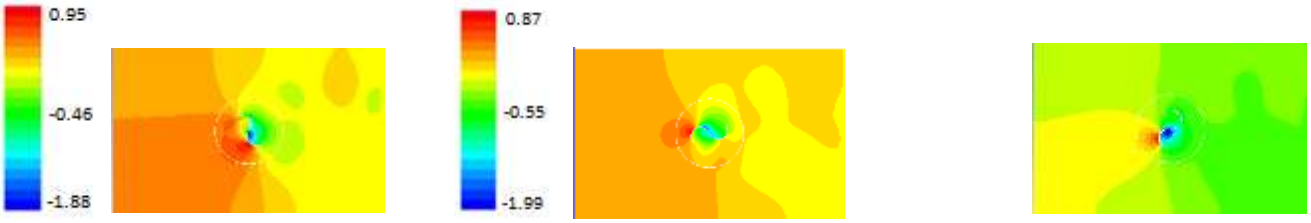


Fig. 6: The pressure coefficient at different calculation times for wind velocity 6 m/s

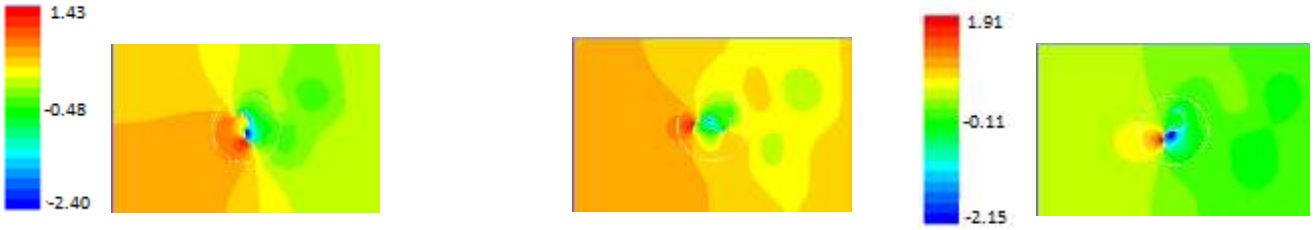


Time = 0.2 s Time =0.4 s Time =0.6 s

Fig. 7: The pressure coefficient at different calculation times for wind velocity 8 m/s

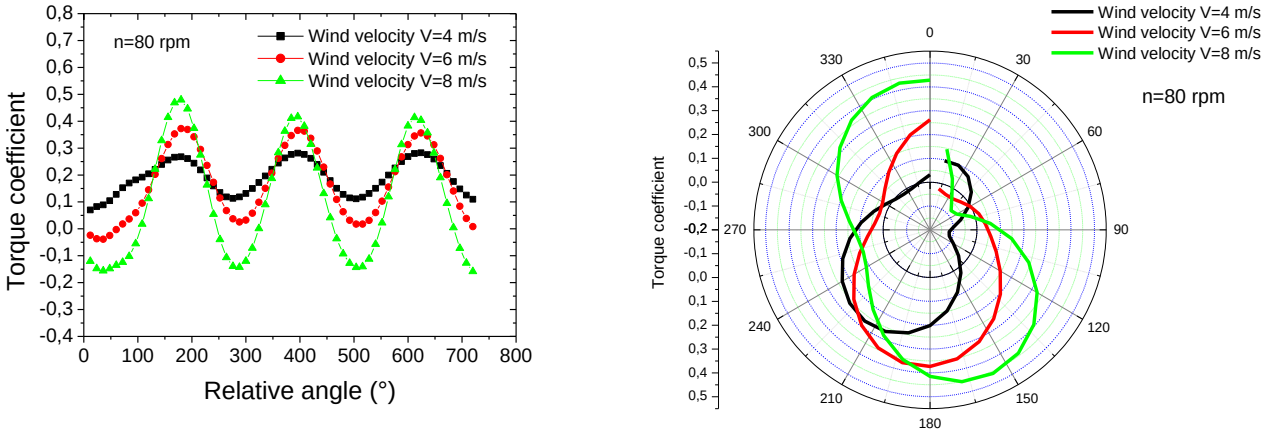


Fig. 8: Torque coefficient for different flow wind velocity (4, 6 and 8 m/s)

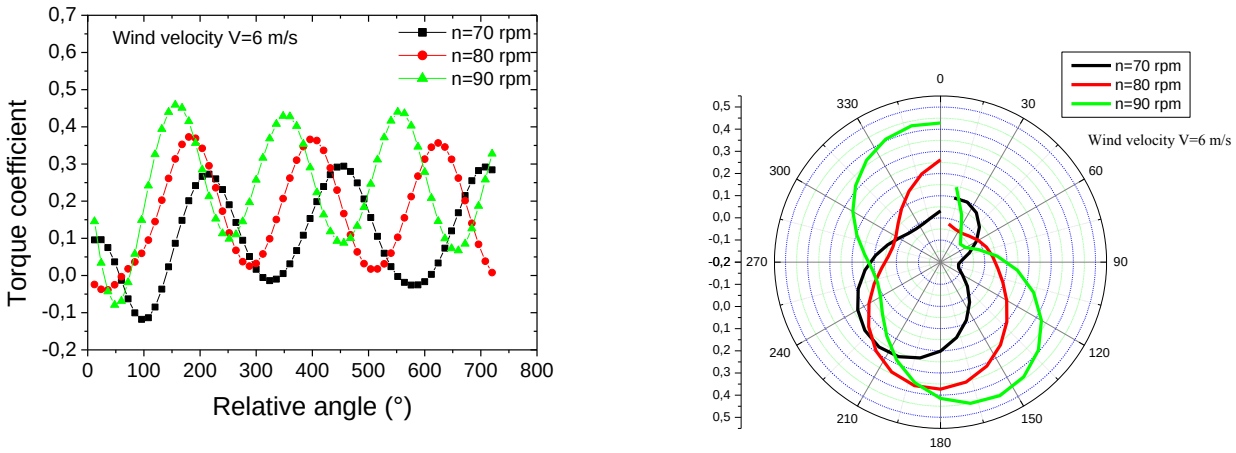


Fig. 9: Torque coefficient for different rotor velocity (70, 80 and 90 rpm)

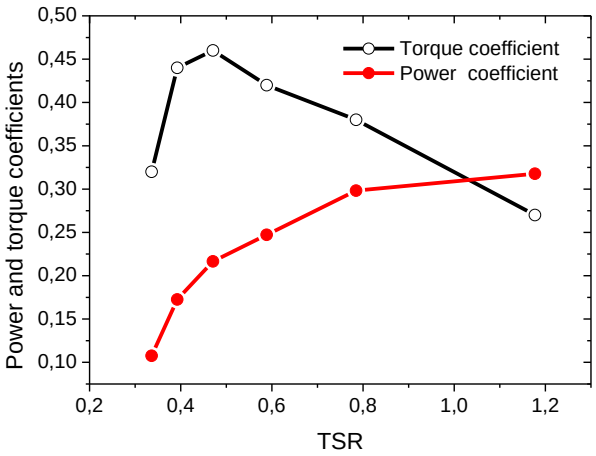


Fig. 10: Power and Torque coefficients for various Tip speed ratio (TSR)

Figure 10 shows the Power and Torque coefficients for various Tip velocity ratios (TSR). We observe in this figure that the optimal point of the torque coefficient is obtained at 0.43 TSR with a value of 0.46. The wind turbine can generate a maximum power coefficient at Cp=0.31 to 1.2 TSR

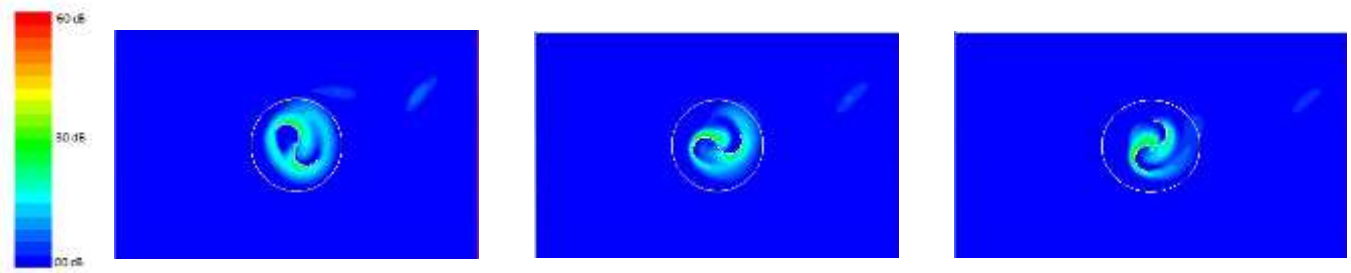

Time = 0.2 s Time =0.4 s Time =0.6 s

Fig. 11: The acoustic power level at different calculation times for wind velocity 4 m/s

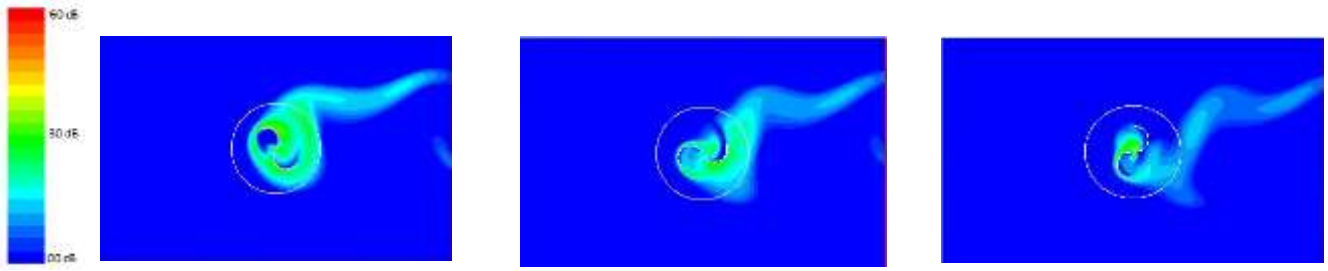

Time = 0.2 s Time =0.4 s Time =0.6 s

Fig. 12: The acoustic power level at different calculation times for wind velocity 6 m/s

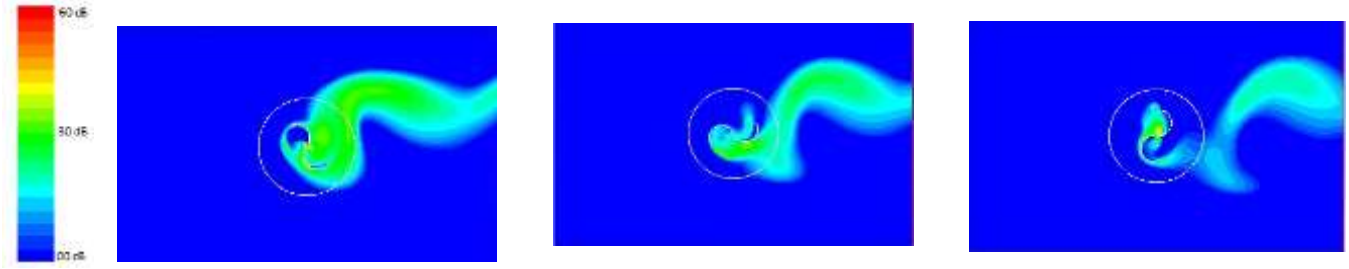

Time = 0.2 s Time =0.4 s Time =0.6 s

Fig. 13: The acoustic power level at different calculation times for wind velocity 8 m/s

## 6 Conclusion

In this study, an unsteady numerical simulation was carried out with the CFD code to understand the aerodynamic and acoustic behavior during the operation of a vertical axis wind turbine of the Savonius type. The results indicate that the torque coefficient depends only on the wind velocity and the rotational velocity angle of the Savonius turbine. The Savonius wind turbine has fairly low torques with maximum and minimum amplitudes with a positive and negative value; these values depend essentially on the rotational velocity angle. In this study the torque coefficient is positive for the intervals angle situated between 120° to 240° and negative for the angles situated between 0° to 100°, 280° to 360°. For acoustic power it is observed that the acoustic power is mainly concentrated at the level of the blades of the Savonius turbine and mainly in the upper part of the blades, this acoustic power is very low the order of 30 dB for a very low wind velocity in occurrence for 4 m/s, the sound field increases according to the increase in wind velocity and according to the orientation of the blades of the wind turbine. We note that this acoustic power strongly depends on the angle of orientation of the blades

The next future work will be on the aero-acoustics of vertical-axis turbines with different blade shapes and different positions.

*References:*

[1] Sebastian Torres, Agustín Marulanda, Miguel F, Montoya, Camilo Hernandez, Geometric design optimization of a Savonius wind turbine, *Energy Conversion and Management* 262, 2022, pp 115679.

[2] Kaya A F, Acir A, Kaya E, Numerical investigation of wind-lens combinations for improving aerodynamic performance of an elliptical-bladed Savonius wind turbine, *J Braz. Soc. Mech. Sci. Eng. 45*, 309, 2023. https://doi.org/10.1007/s40430-023-04216-8.

[3] Umesh K Patel, Nur Alom, Ujjwal K Saha, Aerodynamic analysis of a 2-stage elliptical-bladed Savonius wind rotor: Numerical simulation and experimental validation, *International Journal of Green Energy*, 21:1, 2024, 102-115

[4] Al-Ghriybah M, Lagum, A A, Enhancing the Aerodynamic Performance of the Savonius

Wind Turbine by Utilizing Quarter Elliptical Supplementary Blades, *Flow Turbulence Combust,* 112, 2024, pp.491–508, https://doi.org/10.1007/s10494-023-00516-0.

[5] Dominicus Danardono Dwi Prija Tjahjana, Zainal Arifin, Suyitno Suyitno, Wibawa Endra Juwana, Aditya Rio Prabowo, Catur Harsito, Experimental study of the effect of slotted blades on the Savonius wind turbine performance, *Theoretical and Applied Mechanics Letters*, Vol. 11, Issue 3, 2021, 100249.

[6] Minh Banh Duc, Hung Tran The, Khiem Pham Van, Anh Dinh Le, Predicting aerodynamic performance of savonius wind turbine: An application of generalized k-ω turbulence model, *Ocean Engineering*, Vol. 286, Part 2, 2023, 115690.

[7] Vasileios, Chasiotis, Nikolaos, Tachos, Andronikos, Filios, Computational performance analysis of a two-slotted bucket Savonius rotor. *WSEAS Transactions on Fluid Mechanics*, 2022, vol. 17, p. 49-59, https://doi.org/10.37394/232013.2022.17.5.

[8] M H Pranta, M S Rabbi, M M Roshid, A computational study on the aerodynamic performance of modified savonius wind turbine, *Results in Engineering*, Vol. 10, 2021, 100237

[9] Mu, Zhongqiu, Guoqiang Tong, Zhenjun Xiao, Qingyue Deng, Fang Feng, Yan Li, and Garrel Van Arne, Study on Aerodynamic Characteristics of a Savonius Wind Turbine with a Modified Blade" *Energies* 15,18, 2022, 6661.

[10] Marco Torresi, Fabio A, De Benedittis, Bernardo, Fortunato, Sergio M, Camporeale, Performance and Flow Field Evaluation of a Savonius Rotor Tested in a Wind Tunnel, *Energy Procedia*, Vol. 45, 2014, pp. 207-216.

[11] Dobrev I, Massouh F, Exploring the flow around a Savonius wind turbine. In Proceedings of the 16th *International Symposium on Applications of Laser Techniques to Fluid Mechanics Lisbon, Portugal* 2012.

[12] Sukanta Roy, Ujjwal, K Saha, Wind tunnel experiments of a newly developed two-bladed Savonius-style wind turbine, *Applied Energy*,Vol. 137, 2015, pp. 117-125

[13] Shoutu Li, Qin Chen, Ye Li, Stefan Pröbsting, Congxin Yang, Xiaobo Zheng, Yannian Yang, Weijun Zhu, Wenzhong Shen, Faming Wu, Deshun Li, Tongguang Wang, Shitang Ke, Experimental investigation on noise characteristics of small scale vertical axis wind turbines in urban environments, *Renewable Energy*, Vol. 200, 2022, Pages 970-982.

[14] Livia Brandetti, Francesco Avallone, Delphine De Tavernier, Bruce LeBlanc, Carlos Simão Ferreira, Damiano Casalino, Assessment through high-fidelity simulations of a low-fidelity noise prediction tool for a vertical-axis wind turbine, *Journal of Sound and Vibration*, Vol. 547, 2023, 117486,

[15] N Curle, the Influence of Solid Boundaries upon Aerodynamic Sound. Proceedings of the Royal Society of London. Series A, *Mathematical and Physical Sciences*, 231, 1955, pp. 505-514.

**Contribution of Individual Authors to the Creation of a Scientific Article (Ghostwriting Policy)**

The author contributed in the present research, at all stages from the formulation of the problem to the final findings and solution.

**Sources of Funding for Research Presented in a Scientific Article or Scientific Article Itself**

No funding was received for conducting this study.

**Conflict of Interest**

The author has no conflicts of interest to declare